Pure Appl. Chem., Vol. 79, No. 10, pp. 1653–1673, 2007.
doi:10.1351/pac200779101653

Enthalpies of formation and lattice parameters of B2 phases in Al–Ni–X systems*

Rongxiang Hu, Hsin-Ning Su, and Philip Nash‡

Thermal Processing Technology Center, Illinois Institute of Technology (IIT), 10 West 32nd Street, Chicago, IL 60616, USA

Abstract: Enthalpies of formation of Al–Ni–X (X: Fe, Ru, Pd, Pt, and Cu) alloys were measured by high-temperature calorimeter and compared with the calculated value from Miedema's model and interpolation models. The interpolation models generally provide better prediction than Miedama's model. No one interpolation model generated superior predictions. Lattice parameters of B2 phase compounds were determined by X-ray diffraction (XRD). The atomic volumes in the Al–Ni–Fe system were calculated and show that Fe substitutes preferentially on the Al sublattice. The heat content of $Al_{0.5}Ni_{0.2}Ru_{0.3}$ and $Al_{0.5}Ni_{0.35}Cu_{0.15}$ at high temperature was obtained, and the results are in good agreement with those heat capacities estimated by the Neumann–Kopp rule.

Keywords: Al–Ni–X alloys; Miedema's model; Neumann–Kopp rule; enthalpies of formation; B2 phase compounds; Al–Ni–Fe.

INTRODUCTION

The Al–Ni–X systems (where X is a third element) are of importance not only because of the Al- and Ni-base alloys, but also because they contain ternary compounds with interesting properties. One of the more interesting compounds that frequently appears in these systems is the B2, CsCl type. There are a large number of binary and ternary intermetallic compounds with the B2, CsCl structure [1], many of which exist over substantial composition ranges [1,2]. The B2 structure has a primitive cubic Bravais lattice with two atoms per unit cell. In the binary compounds, the unit cell contains one atom of each type and so we can consider the lattice to consist of two interpenetrating simple cubic lattices, α and β, each of which contains atoms of only one type under conditions of perfect order at 0 K. A subset of the B2 compounds, the aluminides, where one of the major components is Al and the other is generally a transition-metal (TM) element, are of interest for use in high-temperature structural applications because of their low densities, high melting points, and oxidation resistance [3–5]. Despite these useful properties, the aluminides still present considerable challenges for such applications, in particular, they exhibit poor room-temperature ductility and creep resistance [6,7]. Alloying can be used to modify these properties, and consequently a knowledge of the phase equilibria and thermodynamics of ternary and higher-order systems containing B2 phases is needed [8,9]. Over the last 25 years, there have been many papers dealing with different aspects of binary and ternary B2 compounds. These include phase equilibria [10], thermodynamics [11–13], defect structures [14–16], and mechanical properties [3,17]. Investigations have been both experimental [18,19] and theoretical with a number of first-principles cal-

*Paper based on a presentation at the 12th International IUPAC Conference on High Temperature Materials Chemistry (HTMC-XII), 18–22 September 2006, Vienna, Austria. Other presentations are published in this issue, pp. 1635–1778.

‡Corresponding author

culations being performed for this structure [20–22]. The present work is part of a systematic investigation of the thermodynamics and phase equilibria of Al–Ni–X ternary systems with the third element generally either a TM or rare earth. The work is aimed at populating databases for computational thermodynamics, developing an understanding of alloying, and clarifying phase equilibria. In this paper, we mainly address some issues concerning the B2 phases in these systems.

EXPERIMENTAL

Enthalpies of formation

The experimental procedure has been described in detail previously [18]. Briefly, it involves two experiments, the first measures the heat of reaction on dropping a sample of unalloyed elemental powders which react in the calorimeter and the second the heat content of the reacted sample. The samples are dropped from room temperature (298 K), the difference between the two gives the heat of formation at 298 K. Thus, the standard enthalpy of formation, $\Delta H_f^{298\ K}$ is

$$\Delta H_f^{298\ K} = \Delta H_{reaction} - \Delta H_{heat\ content}$$

A precise knowledge of the temperature of the calorimeter is, in principal, not necessary except in the sense that it must be the same for both experiments. The main experimental issues with this technique are that the sample should react completely in the calorimeter and that on cooling to room temperature, no phase separation should occur, that is, it is single phase at room temperature. Note also that the actual state of the sample at the calorimeter temperature is not important only that it is the same for both experiments. The presence of a liquid phase at the calorimeter temperature is not a problem unless it leads to phase separation, or inhomogeneity in the sample. For example, compounds forming by a peritectic reaction with a melting point below the calorimeter temperature cannot be measured.

Lattice parameters

Lattice parameters of Al–Ni–X B2 compounds are an indirect measure of the bond strength and constitutional defect structure, and can be used to determine the atomic volume of each constituent element.

X-ray diffraction (XRD) was performed in a ThermoARL diffractometer using Cu Kα radiation. Scans were taken over a 2θ range of 5 to 120°. The "1976 XRD Flat-Plate Intensity Standard" alumina purchased from NIST (National Institute of Standards and Technology) is used as the standard reference material for calibration to obtain precise peak positions and accurate lattice parameters.

Once the calibration curve is obtained, the peak position obtained from subsequent experiment has to be corrected by the equation of the calibrated curve. Several index planes in an XRD pattern were used to determine the lattice parameter by an extrapolation function [23].

B2 Compounds

One of the interesting aspects of the B2 structure is the existence of constitutional crystal defects when the composition deviates from the stoichiometric composition. In the fully ordered stoichiometric compound, one type of atom occupies the α-sublattice and the other type of atom the β-sublattice. This occurs only at 0 K, but at finite temperatures thermal defects are present in increasing number as the temperature is increased. We will ignore for the most part the presence of such thermal defects since our discussion will focus on room-temperature and sufficiently large deviations from stoichiometry that thermal defects constitute a small fraction of the total. When there are no longer equal numbers of the two atoms the structure must introduce some type of atomic defect to maintain the crystal structure. While several types of defect are possible, experience has shown that the most common defects are TM antistructure atoms on the Al-sublattice for composition deviations to the TM side and vacancies on the

TM sublattice when there is an Al excess. When adding the third element X to NiAl, the site preference of the third element can be predicted from the enthalpies of formation of NiX and AlX [39], as shown in Table 1. At stoichiometry, it is possible to have TM antistructure atoms on the Al sublattice with two vacancies on the TM sublattice to maintain the equality of lattice sites, so-called triple defects [24].

Table 1 The calculated K value and the preference of X in Al–Ni–X B2 systems.

Dilute addition C	ΔH^{f}_{CAl} (kJ/mol)	ΔH^{f}_{NiC} (kJ/mol)	K (kJ/mol)	Relative site preference compared to Ni	Absolute site preference of infinitesimal addition at 298 K
Sc	–41.1 ± 1.5 [27]	–44.7 ± 2.3 [35]	73.1	β	
Ti	–38 [28]	–33.1 ± 1.1 [36]	64.6	β	
Mn	–21.55 ± 1.05 [29] (898 K)	–14.21 [28] (1050 K)	62.16	β	
Fe	–26.5 ± 1.1 [18]	–3.86 [28] (1200 K)	46.86	β	
Co	–53.4 ± 1.4 [27]	0 [28] 1400 K	16.1	β	
Ni	–62 ± 2 [30]	0	7.5		
Cu	–20.04 [29]	1.8 [28] 973 K	47.66	β	
Y	–88 [31]	–37 [37]	18.5	β	
Ru	–62.05 ± 1.6 [32]	+1 [34] cal.	6.45	β	
Ru	–54.5 ± 1.2 [19]	+1 [34] cal.	14	β	
Rh	–106.3 ± 1.6 [32]	+1.1 [38] 1100 K	–37.9	α	α
Pd	–91.25 ± 4.7 [33]	–0.5 [28] 1273 K	–21.25	α	α
Re	–30 [34]	+3 [34] cal.	36.5	β	
Os	–38.6 ± 0.9 [32]	+2 [34] cal.	28.9	β	
Ir	–92.8 ± 1.8 [32]	–2 [34] cal.	–21.3	α	α
Pt	–97.55 ± 5 [33]	–9.3 [28]	–18.75	α	α

$K = \Delta H^{f}_{CB} - \Delta H^{f}_{AB} - \Delta H^{f}_{AC} - \Delta H^{bcc\rightarrow fcc}_{Ni} = \Delta H^{f}_{CAl} - \Delta H^{f}_{AlNi} - \Delta H^{f}_{NiC} - \Delta H^{bcc\rightarrow fcc}_{Ni}$
$\Delta H^{bcc\rightarrow fcc}_{Ni} = 7.99$ kJ/mol.
Relative site preference: $K > 0 \rightarrow C$ has a stronger preference for β-sublattice (Al); $K < 0 \rightarrow C$ has a stronger preference for α-sublattice (Ni).
Absolute site preference: $K < 0 \rightarrow C$ has a stronger preference for α-sublattice.

The enthalpy of formation of a B2 compound reflects the total bond strength resulting from the formation of unlike atom bonds, and in the case of non-stoichiometric alloys will also include some other bonds such as like atom bonds or vacancy-atom bonds. Thus, if we measure the enthalpy of formation as a function of composition we expect it to vary in accordance with the changes in numbers of bonds of each type. The experimental error involved in determination of enthalpies of formation means that sensitivity is limited and therefore significant compositional variations are needed to obtain useful information on the constitutional defect structure. One example of such measurements is for the compositional variation of the enthalpy of formation of NiAl [12]. The enthalpy of formation is a maximum

at the stoichiometric composition and decreases at different rates on the Al- and Ni-rich sides. This is a consequence of the different constitutional defect structures, with antistructure atoms on the Ni-rich side replacing Al–Ni bonds with weaker Ni–Ni bonds and weaker Al-vacancy bonds on the Al-rich side. Since the Al atom is significantly larger than Ni, there is a compositional variation of the lattice parameter, which also depends on the types of defect formed [6]. Furthermore, there is a significant effect on hardness due to the strain effects resulting from the different defects [25,26].

At the stoichiometric composition, the effect of adding a third element to AlNi would be to change the enthalpy of formation toward the value for the aluminide of the added element. Deviation from a linear relationship would indicate a second near-neighbor effect between the third element and Ni. This effect will most likely be small if the third element is a TM. There may also be a change in the number of thermal defects if the third element has a site preference, but we are assuming small concentrations at 298 K for the purpose of this discussion. However, as one moves away from stoichiometry to Al-deficient compositions the interaction between the third element and Ni becomes important in determining site preference, and this determines the number and types of bonds formed. The effect becomes more pronounced as the Al content decreases because the probability for forming nearest-neighbor Ni–Ni bonds or Ni–X bonds increases as the Ni and/or third element must make up the deficiency on the Al sublattice.

A number of models have been developed for the description of the thermodynamic properties of B2 phases usually using a Bragg–Williams (B–W) or Wagner–Schottky (W–S) formalism [13,18,39]. These models are useful for making predictions of defect concentrations and for providing the thermodynamic description of the phase for computational thermodynamics databases. An excellent review on this topic was written by Chang and Neumann [40]. Since then, additional experimental data have become available, in particular, enthalpy of formation, lattice parameter, and defect concentrations [18,19,26].

RESULTS AND DISCUSSION

Al–Ni–Fe

Experimental enthalpies of formation were compared to Miedema's semiempirical model [41] and the interpolation methods of Toop, Kohler, Colinet, Muggianu, and Hillert [42].

Using the extended Miedema model [41], the standard enthalpy of formation of a ternary compound, $\Delta H_f^{298\ K}$, can be calculated from

$$\Delta H_f^{298\ K} = C_A f_B^A \Delta H_{(AinB)}^{inter} + C_A f_C^A \Delta H_{(AinC)}^{inter} + C_B f_C^B \Delta H_{(BinC)}^{inter}$$

C_A and C_B are the molar ratios of A and B elements, respectively, in the corresponding compounds, f_B^A is the degree of surface contact of an A atom with B neighbors while f_C^A is the degree of surface contact of an A atom with C neighbors. ΔH^{inter} is interfacial enthalpy.

Hillert [42] has classified the empirical models for the prediction of enthalpies of formation in ternary systems into two categories depending on the method of choosing the binary composition:

- symmetric model: Kohler [43], Colinet [44], and Muggianu [45]
- asymmetric model: Toop [46] and Hillert [42]

They are shown in Fig. 1.

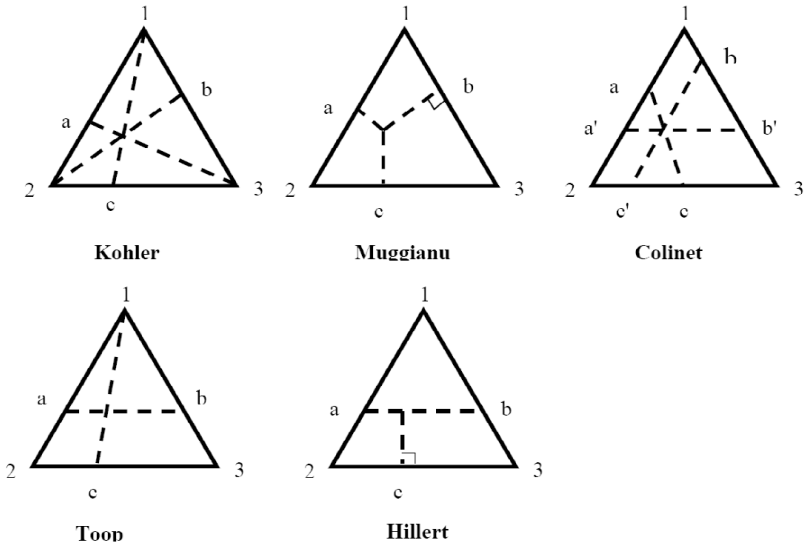

Fig. 1 Interpolation models for predicting ternary enthalpies of formation.

Figures 2–4 show the comparison of experimental enthalpies of formation at 298 K with empirical interpolations and Miedema's model in the Al–Ni–Fe system. f^{A}_{B}, f^{A}_{C}, f^{B}_{C}, ΔH^{inter}_{AinB}, ΔH^{inter}_{AinC}, and ΔH^{inter}_{BinC} values for Miedama's model are from [41]. The enthalpies of formation of binary compounds for the interpolation models are from [34] with some additions, Table 2. It is apparent that enthalpies calculated from Miedema's model are less exothermic than those measured from direct synthesis calorimetry, but both show the same tendency of enthalpy change with composition. The interpolation models provide very reasonable approximations to the experimental values in most cases.

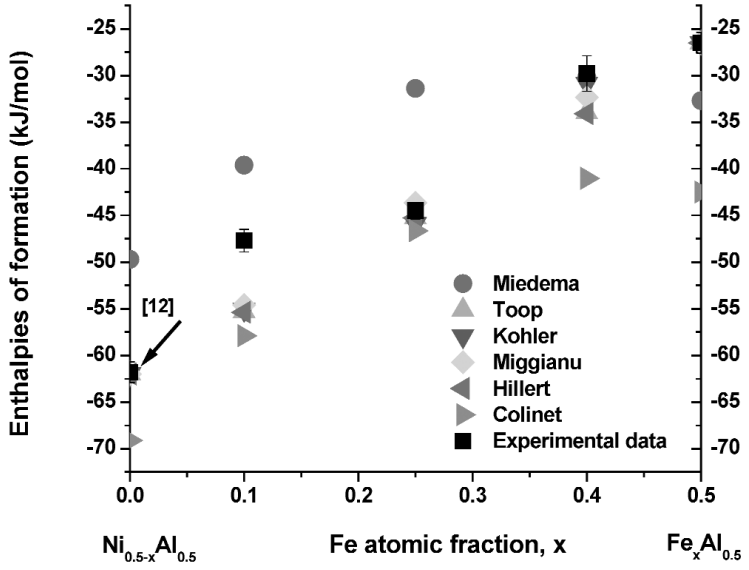

Fig. 2 Comparison of experimental enthalpies of formation at 298 K with empirical interpolations and Miedema's model for $Al_{0.5}Ni_{0.5-x}Fe_x$.

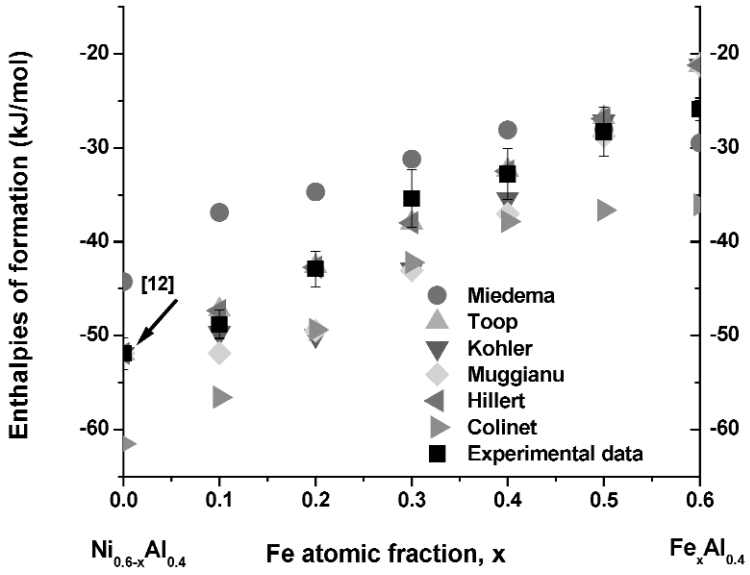

Fig. 3 Comparison of experimental enthalpies of formation at 298 K with empirical interpolations and Miedema's model for $Al_{0.4}Ni_{0.6-x}Fe_x$.

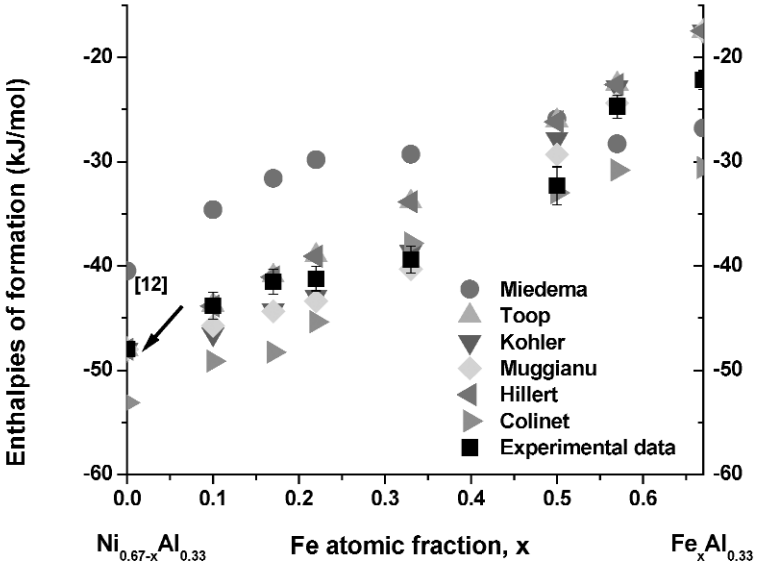

Fig. 4 Comparison of experimental enthalpies of formation at 298 K with empirical interpolations and Miedema's model for $Al_{0.33}Ni_{0.67-x}Fe_x$.

Table 2 ΔH_{Al-X} and ΔH_{Ni-X} at 298 K [34] (kJ/mol).

		Ni	Co	Pd	Pt	Fe	Ru
	Al_9X_2		–30				
	Al_4X				–57		
	$Al_{13}X_4$		–32				
	Al_3X	–38	–38	–51*		–28	
	Al_5X_2		–41			–25	
	Al_2X					–26	
	Al_3X_2	–57		–84*	–96.5 [47]		
Al–X	AlX	–62 [30]	–53.4 [27]	–91.25 [33]	–97.6 [33]	–26.5 [18]	–54.5 [19]
	Al_2X_3				–86		
	Al_3X_5				–89		
	AlX_2			–87.3 [48]			
	AlX_3	–41			–63.6 [47]		
Ni–X	$Ni_{0.5}X_{0.5}$	0	0	–0.5 (1273 K)	–9.3	–4 [49]	+1

*373 K.

Figure 5 shows a Gibbs triangle with experimentally determined enthalpies of formation of the B2 phase [18] superimposed with the B2 phase boundaries at 1400 K [50]. Although the calorimeter samples were slowly cooled to room temperature from the calorimeter temperature, they show that the B2 phase field in Al–Ni–Fe is more extensive than predicted by the thermodynamic model of [50]. Measurements of the composition dependence of the lattice parameter of the B2 phase have also been made [51]. Figure 6 shows the composition dependence of the lattice parameter of the B2 phase in Al–Ni–Fe for constant Al content of 0.4 [51]. It is clear there is a change of slope that occurs at 0.1 Fe for the $Al_{0.4}Ni_{0.6-x}Fe_x$. Similar results have been obtained by Pike et al. [26]. The results clearly indicate that the larger Fe atom preferentially occupies the antistructure sites on the Al sublattice, and only when these are filled do the Fe atoms begin to occupy the TM sublattice. An analysis of these data [51] produced the following atomic volumes in the $Al_{0.40}Ni_{(0.60-x)}Fe_x$ section:

$$V_{Al/Al} = 0.0134 \text{ nm}^3$$

$$V_{Ni/Al} = 0.0107 \text{ nm}^3$$

$$V_{Ni/Ni} = 0.0106 \text{ nm}^3$$

$$V_{Fe/Al} = 0.0131 \text{ nm}^3$$

$$V_{Fe/Ni} = 0.0112 \text{ nm}^3$$

Similar values are obtained for constant 0.33 mole fraction Al.

The atomic volumes of the atoms indicates that the constitutional defect site preference of Fe for the Al sublattice is due to the closer match of the Fe atomic volume with that of the Al coupled with the lower bond strength of Al–Fe. Hardness measurements of [26] also indicate such a site preference, and the softening observed on adding Fe results from the smaller lattice strain than for Ni.

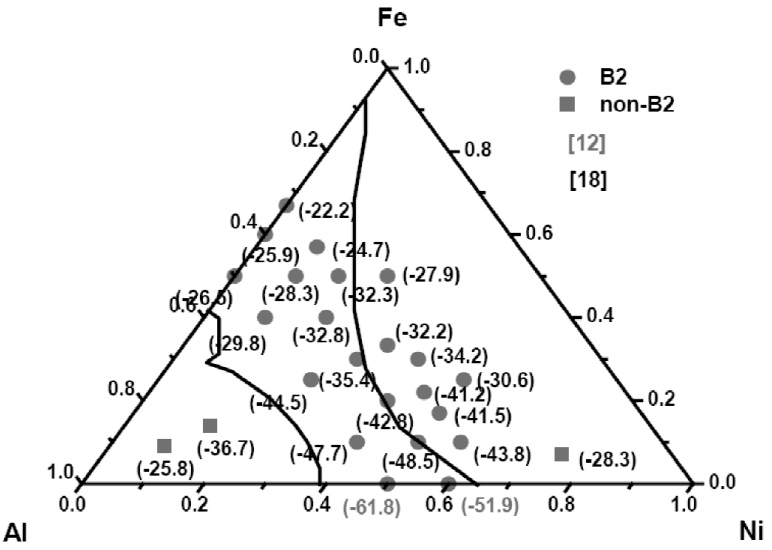

Fig. 5 Enthalpies of formation of B2 compounds in the Al–Ni–Fe system [18] and B2 phase boundary at 1400 K [50].

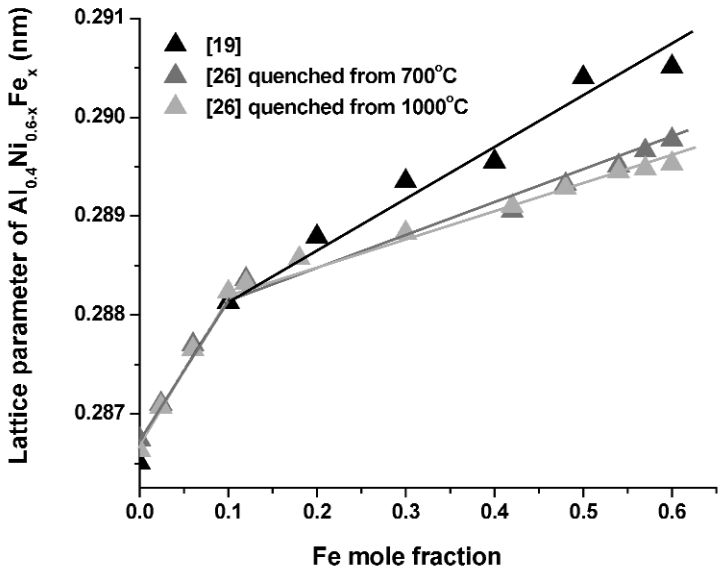

Fig. 6 Lattice parameter of $Al_{0.4}Ni_{0.6-x}Fe_x$.

The composition dependence of ΔH_f of the B2 phase in the Al–Ni–Fe system using the W–S model is

$$\Delta H_f = \Delta H^*(1 + x_{20}) + \Delta H_{12}x_{12} + \Delta H_{13}x_{13} + \Delta H_{20}x_{20} + \Delta H_{21}x_{21} + \Delta H_{23}x_{23}$$

$$\Delta H^* = x\Delta H^f_{NiAl} + (1 - x)\,\Delta H^f_{NiAl}$$

The definitions of the parameters in the above equations are given in Table 3. Table 4 shows the enthalpy coefficients in the W–S model.

Table 3 Definitions of the parameters in the W–S model of the B2 phase.

Parameter	Definition
ΔH^{f}	Enthalpy of formation of B2 phase in Al–Ni–Fe
ΔH^{*}	Enthalpy of formation of 1 mole of the ideally stoichiometric B2 phase
ΔH_{12}	Enthalpy of formation of 1 mole of Ni antistructure atoms in the β-sublattice
ΔH_{13}	Enthalpy of formation of 1 mole of Fe antistructure atoms in the β-sublattice
ΔH_{20}	Enhthalpy of formation of 1 mole of vacancies in the α-sublattice
ΔH_{21}	Enthalpy of formation of 1 mole of Al antistructure atoms in the α-sublattice
ΔH_{23}	Enthalpy of formation of 1 mole of Fe in the α-sublattice
x_{12}	Concentration of Ni antistructure atoms in the β-sublattice
x_{13}	Concentration of Fe antistructure atoms in the β-sublattice
x_{20}	Concentration of vacancies in the α sublattice
x_{21}	Concentration of Al antistructure atoms in the α-sublattice
x_{23}	Concentration of Fe antistructure atoms in the α-sublattice
ΔH^{f}_{AlNi}	Enthalpy of formation of 1 mole of the ideally stoichiometric AlNi
ΔH^{f}_{AlFe}	Enthalpy of formation of 1 mole of the ideally stoichiometric AlFe

Table 4 Enthalpy coefficients in the W–S model of the B2 phase in Al–Ni–Fe.

Enthalpy coefficients	kJ/mol
ΔH_{12}	97.5 (AlNi) [12]
ΔH_{13}	70.3 (AlFe) [54]
ΔH_{23}	–15.8 ($Al_{0.33}Ni_{(0.67-x)}Fe_x$) [18]
ΔH_{23}	0 ($Al_{0.50}Ni_{(0.50-x)}Fe_x$) [18]
ΔH_{23}	~0 ($Al_{0.40}Ni_{(0.60-x)}Fe_x$) [18]

The data, Figs. 2–4, show that ΔH_{23} is small (0–2 kJ/mol) for the 0.5 and 0.4 Al sections but for the 0.33 section ΔH_{23} = –15.8 kJ/mol consistent with a small negative heat of mixing of Fe and Ni [18]. As discussed previously, the Ni–X bond strength will be more influential on the enthalpies of formation the smaller is the Al concentration since the probability of such bonds increases with decreasing Al content.

Al–Ni–Ru

Some controversy exists regarding the existence of a miscibility gap in this system in the extensive B2 phase field extending from NiAl to RuAl [52,53]. If there is a miscibility gap then the critical temperature is likely relatively low, resulting in a kinetic constraint on the phase separation, making experimental verification quite difficult. Calorimetric data on enthalpies of formation at 298 K indicate unusual behavior, Fig. 7, where there is a decrease in the enthalpy of formation of the B2 compound around 0.1 mole fraction of Ru, indicating a reduction in stability which will likely result in a miscibility gap, very different from the values predicted by Hillert interpolation model. The effect diminishes on reducing the Al concentration below stoichiometry [19]. This results in negative curvatures for the enthalpy–composition relation characteristic of systems exhibiting miscibility gaps. Since at equilibrium it appears probable that there is a miscibility gap, then some of the experimental data on enthalpy of formation of the B2 phase obtained in our work represents the metastable enthalpy curve, XRD on the samples shows only one B2 phase [19]. At 298 K, we should have phase separation but this did not occur because the transformation is kinetically constrained.

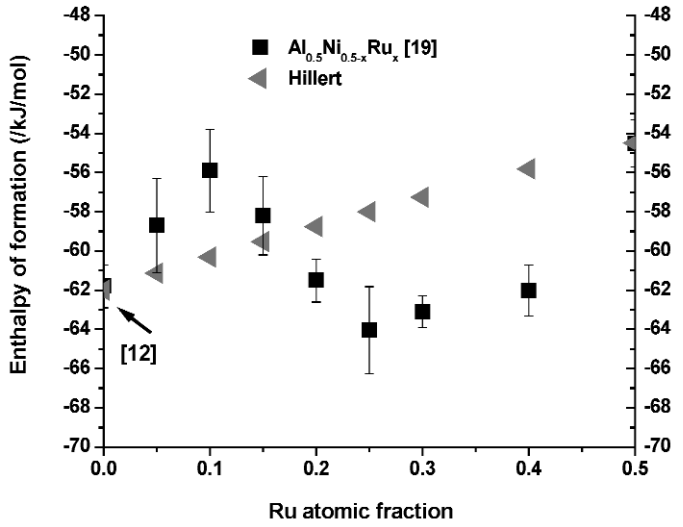

Fig. 7 Enthalpies of formation of $Al_{0.50}Ni_{0.50-x}Ru_x$ [19].

Heat content and capacity

The heat content of $Al_{0.5}Ni_{0.2}Ru_{0.3}$ between room temperature and high temperatures (from 1243 to 1470 K) was measured, and its heat capacity was calculated over this temperature range by fitting the heat content linearly, Fig. 8. The calculated value of C_p = 27.2 J/mol/K, which is close to the value of 32.4 J/mol/K estimated using the Neumann–Kopp rule and slightly lower than the value for $Ni_{0.5}Al_{0.5}$, which is about 30.5 J/mol/K. This is reasonable since the heat capacity of Ru is smaller than Ni in this temperature range.

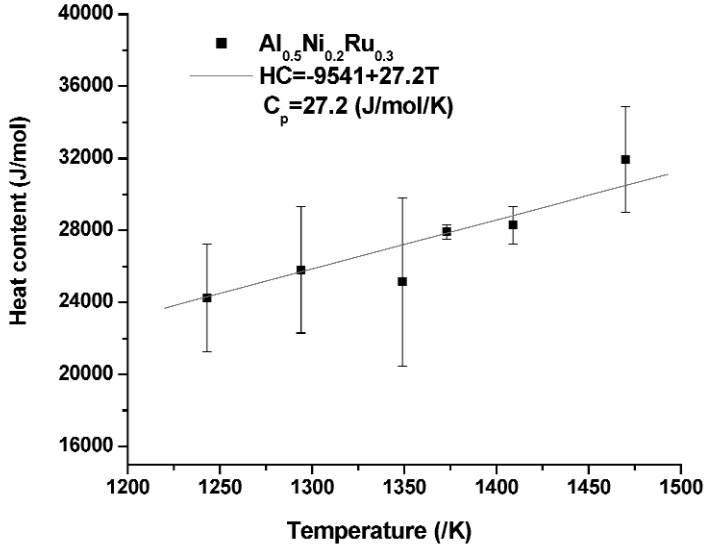

Fig. 8 Heat content and heat capacity of $Al_{0.5}Ni_{0.2}Ru_{0.3}$ at high temperature.

Al–Ni–Pt

The enthalpies of formation of the Al–Ni–Pt phases, B2, $L1_2$, Al_3Ni_2, (Al) and (Ni, Pt) are shown in Fig. 9, superimposed with the B2 phase boundaries at 1333K [55]. With constant Al, when replacing Ni with Pt, the enthalpy of formation of Al–Ni–Pt increases because of the stronger Al–Pt bonding energy. The experimental data are compared with the calculated data from Miedema's model and the interpolation models, Figs. 10–13. The linear enthalpy change with composition from $Ni_{0.5}Al_{0.5}$ to $Pt_{0.5}Al_{0.5}$ indicates the small interaction energy between Ni and Pt, which is in accordance with the enthalpy of formation from [34]. The Miedema predictions are consistently less exothermic than the experimental data, while the interpolation models provide good estimates.

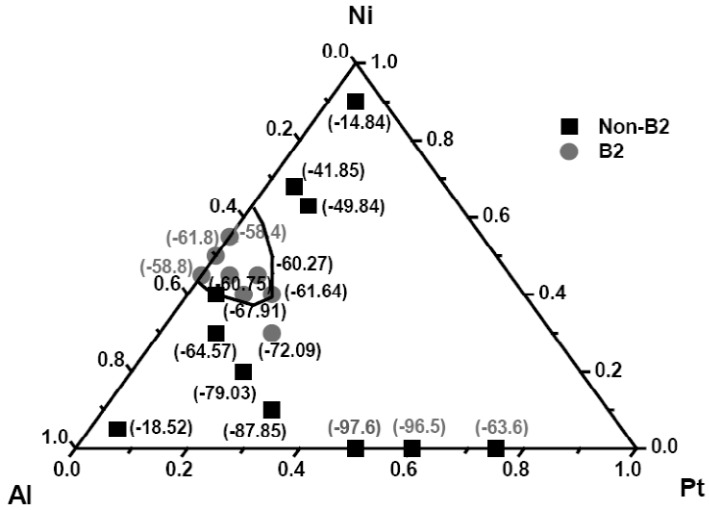

Fig. 9 Enthalpies of formation of Al–Ni–Pt compounds [this work] and B2 phase boundary at 1333 K [55], the binary data points are from [12,33,34,47].

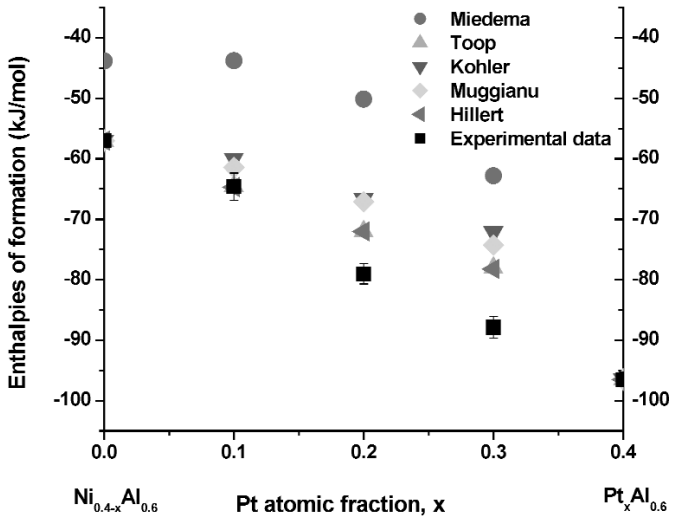

Fig. 10 Comparison of experimental enthalpies of formation at 298 K with empirical interpolations and Miedema's model for $Al_{0.6}Ni_{0.4-x}Pt_x$.

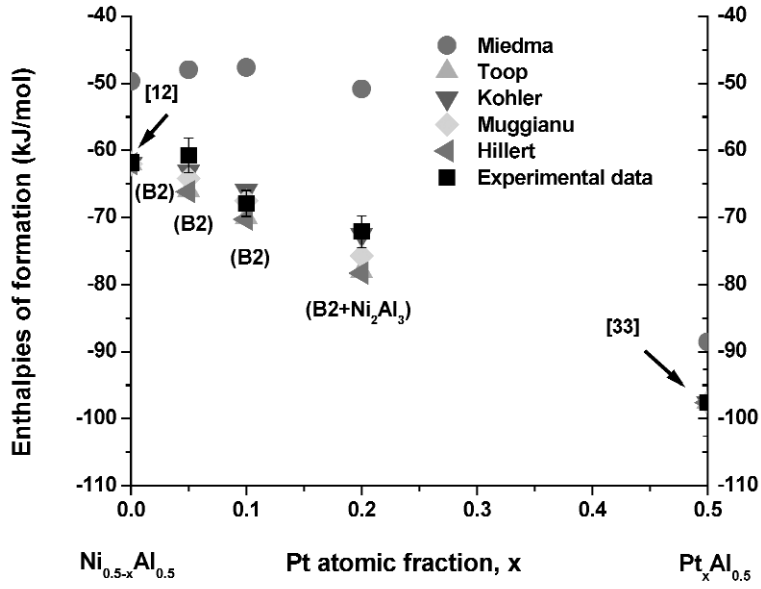

Fig. 11 Comparison of experimental enthalpies of formation at 298 K with empirical interpolations and Miedema's model for $Al_{0.5}Ni_{0.5-x}Pt_x$.

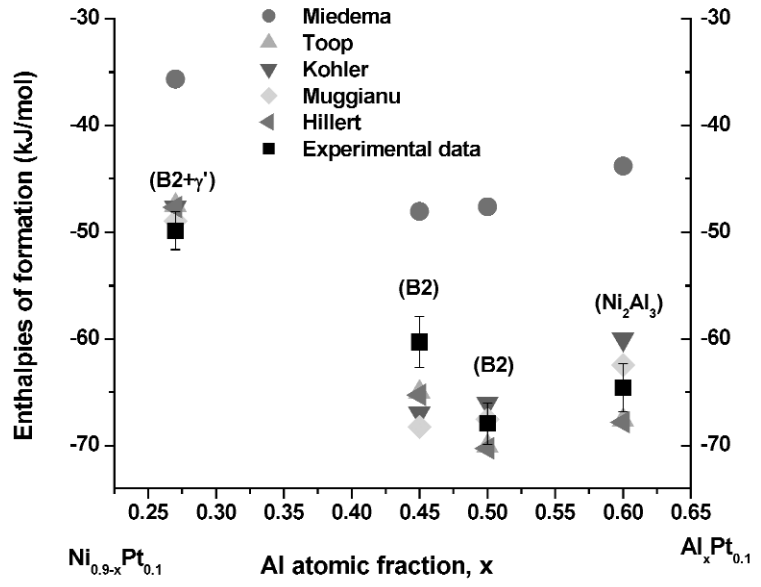

Fig. 12 Comparison of experimental enthalpies of formation at 298 K with empirical interpolations and Miedema's model for $Ni_{0.9-x}Al_xPt_{0.1}$.

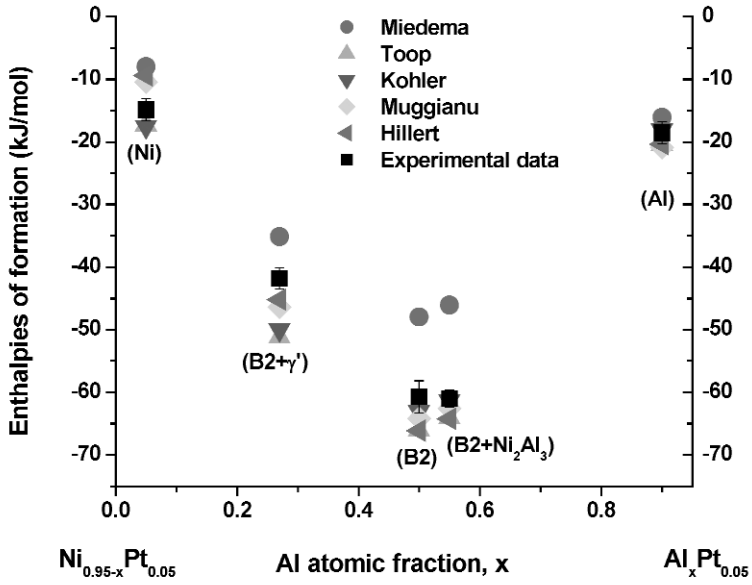

Fig. 13 Comparison of experimental enthalpies of formation at 298 K with empirical interpolations and Miedema's model for $Ni_{0.95-x}Al_xPt_{0.05}$.

XRD was used to determine the crystal structure and phases of each sample, and the results are shown in Table 5. The composition $Al_{0.5}Ni_{0.3}Pt_{0.2}$ shows diffraction peaks from B2 with a small amount of a second phase in agreement with the phase equilibria [55].

Table 5 Phases and lattice parameters of Al–Ni–Pt alloys.

Composition	Reaction enthalpy, ΔH_1 (kJ/mol)	Heat content, ΔH_2 (kJ/mol)	Enthalpy of formation ΔH_f (kJ/mol)	Phase	Lattice parameter of B2 phase (nm)
$Al_{0.5}Ni_{0.5}$			–61.8 ± 1.11 [12]	B2	0.2887
$Al_{0.5}Ni_{0.45}Pt_{0.05}$	–31.04 ± 2.0	29.71 ± 1.33	–60.75 ± 2.59	B2	0.2903
$Al_{0.5}Ni_{0.4}Pt_{0.1}$	–36.04 ± 1.33	31.87 ± 1.05	–67.91 ± 1.93	B2	0.2924
$Al_{0.5}Ni_{0.3}Pt_{0.2}$	–40.62 ± 2.07	31.47 ± 0.71	–72.09 ± 2.38	B2 + ?	0.2963
$Al_{0.45}Ni_{0.45}Pt_{0.1}$	–29.39 ± 1.79	30.88 ± 1.26	–60.27 ± 2.38	B2	0.2915
$Al_{0.45}Ni_{0.4}Pt_{0.15}$	–31.8 ± 0.95	29.84 ± 1.22	–61.64 ± 1.79	B2	0.2939
$Al_{0.5}Pt_{0.5}$			–97.6 ± 5.0 [33]	B2	0.3212 (1545–1613 K) [56]
$Al_{0.4}Ni_{0.6}$			–51.9 ± 1.7 [12]	B2	0.2865 [6]
$Al_{0.55}Ni_{0.4}Pt_{0.05}$	–29.6 ± 0.51	31.39 ± 0.81	–60.99 ± 1.33	B2 + Al_3Ni_2	0.2881
$Al_{0.6}Ni_{0.3}Pt_{0.1}$	–29.68 ± 1.28	34.89 ± 1.54	–64.57 ± 2.23	Al_3Ni_2	–
$Al_{0.6}Ni_{0.2}Pt_{0.2}$	–45.75 ± 1.25	33.28 ± 0.52	–79.03 ± 1.64	Al_3Ni_2	–
$Al_{0.6}Ni_{0.1}Pt_{0.3}$	–57.74 ± 1.27	30.11 ± 0.81	–87.85 ± 1.77	Al_3Ni_2	–
$Al_{0.27}Ni_{0.63}Pt_{0.1}$	–12.29 ± 1.19	37.55 ± 0.96	–49.84 ± 1.79	B2 + $L1_2$	–
$Al_{0.27}Ni_{0.68}Pt_{0.05}$	–5.31 ± 1.16	36.54 ± 0.82	–41.85 ± 1.70	B2 + $L1_2$	–
$Al_{0.05}Ni_{0.90}Pt_{0.05}$	25.12 ± 1.3	39.96 ± 0.71	–14.84 ± 1.75	(Ni, Pt)	–
$Al_{0.9}Ni_{0.05}Pt_{0.05}$	25.33 ± 0.84	43.85 ± 1.26	–18.52 ± 1.77	(Al)	–

Al–Ni–Pd

No ternary phase diagram of the Al–Ni–Pd system is available, so the enthalpies of formation and crystal structures of Al–Ni–Pd compounds were investigated to provide the basic data for developing the phase diagram.

Figure 14 shows that enthalpies of formation of Al–Ni–Pd compounds increase as Pd replaces Ni since the Al–Pd bonds are stronger than Al–Ni bonds. Figure 15 shows that the enthalpies of formation of $Al_{0.5}Ni_{0.5-x}Pd_x$ ($0 \le x \le 0.5$) are linear between $Ni_{0.5}Al_{0.5}$ and $Pd_{0.5}Al_{0.5}$, which indicates a negligible second near-neighbor interaction energy between Ni and Pd.

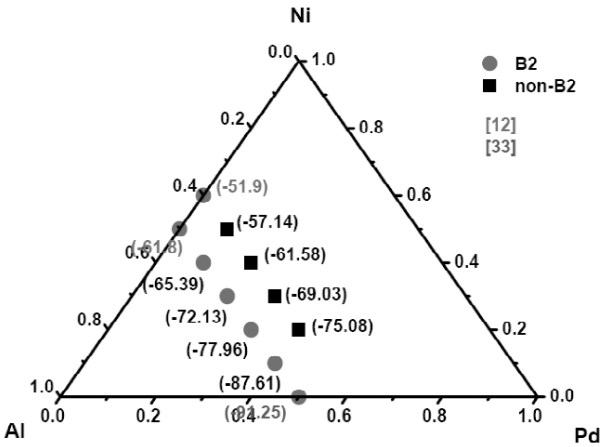

Fig. 14 Enthalpies of formation of Al–Ni–Pd compounds.

Miedema's model predicts less endothermic values for the enthalpies of formation, see Figs. 15 and 16. The empirical models predict the enthalpies of formation quite well with no particular model being generally better than the others.

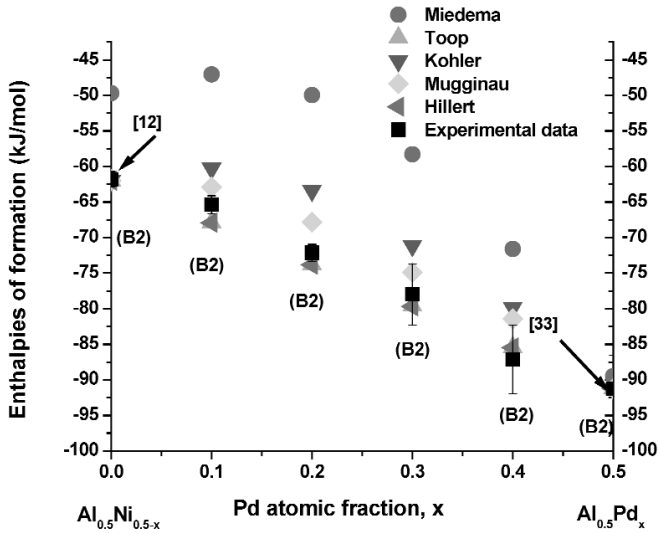

Fig. 15 Comparison of experimental enthalpies of formation at 298 K with empirical interpolations and Miedema's model for $Al_{0.5}Ni_{0.5-x}Pd_x$.

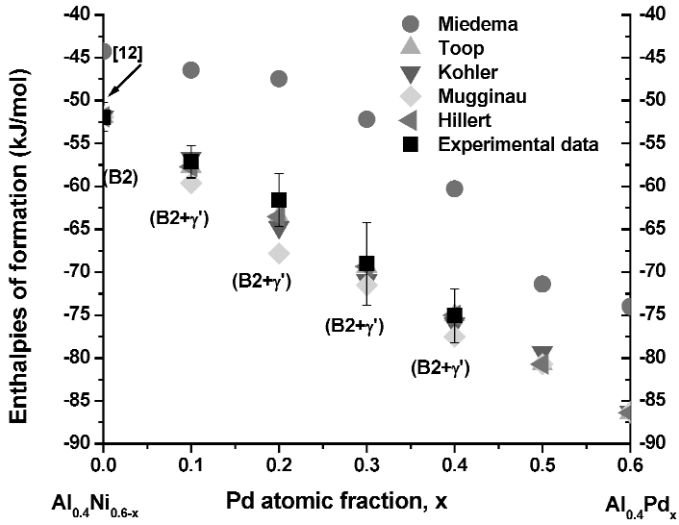

Fig. 16 Comparison of experimental enthalpies of formation at 298 K with empirical interpolations and Miedema's model for $Al_{0.4}Ni_{0.6-x}Pd_x$.

XRD of $Al_{0.5}Ni_{0.5-x}Pd_x$ alloys shows that they are single-phase B2 compound. $Al_{0.4}Ni_{0.6-x}Pd_x$ ($0 < x \leq 0.5$) alloys are within the two-phase region, B2 + $L1_2$. The crystal structures and lattice parameters are summarized in Table 6. The lattice parameters of $Al_{0.5}Ni_{0.5-x}Pd_x$ B2 phase, Fig. 17, show that with x increasing, the lattice parameter increases linearly, which indicates that the Pd simply substitutes for Ni on the Ni-sublattice.

Table 6 Phases and lattice parameters of the Al–Ni–Pd compounds.

Composition	Reaction enthalpy, ΔH_1 (kJ/mol)	Heat content, ΔH_2 (kJ/mol)	Enthalpy of formation ΔH_f (kJ/mol)	Phase	Lattice parameter of B2 phase (nm)
$Al_{0.5}Ni_{0.5}$			–61.8 ± 1.11 [12]	B2	0.2887 [6]
$Al_{0.5}Ni_{0.4}Pd_{0.1}$	–34.35 ± 0.55	31.04 ± 0.8	–65.39 ± 1.26	B2	0.2916
$Al_{0.5}Ni_{0.3}Pd_{0.2}$	–40.45 ± 0.18	31.68 ± 0.87	–72.13 ± 1.19	B2	0.2956
$Al_{0.5}Ni_{0.2}Pd_{0.3}$	–44.44 ± 1.95	33.52 ± 3.75	–77.96 ± 4.30	B2	0.2984
$Al_{0.5}Ni_{0.1}Pd_{0.4}$*	–50.52 ± 3.47	36.64 ± 3.03	–87.16 ± 4.85	B2	0.3001
$Al_{0.5}Pd_{0.5}$			–91.25 ± 4.7 [33]	B2	0.3049 [56]
$Al_{0.40}Ni_{0.60}$			–51.9 ± 1.7 [12]	B2 + $L1_2$	–
$Al_{0.4}Ni_{0.5}Pd_{0.1}$	–20.61 ± 1.25	36.53 ± 1.12	–57.14 ± 1.86	B2 + $L1_2$	–
$Al_{0.4}Ni_{0.4}Pd_{0.2}$	–25.58 ± 1.42	36 ± 2.26	–61.58 ± 3.07	B2 + $L1_2$	–
$Al_{0.4}Ni_{0.3}Pd_{0.3}$	–35.87 ± 3.77	33.16 ± 2.91	–69.03 ± 4.83	B2 + $L1_2$	–
$Al_{0.4}Ni_{0.2}Pd_{0.4}$	–42.56 ± 2.2	32.52 ± 1.51	–75.08 ± 3.1	B2 + $L1_2$	–

*With small amount of non-B2 phase.

The results show that the B2 phase field extends across the ternary system from NiAl to PdAl. However, the B2 phase field does not extend far on the Al-deficient side with all ternary compositions studied at constant $Al_{0.4}$ consisting of B2 + $L1_2$ phases.

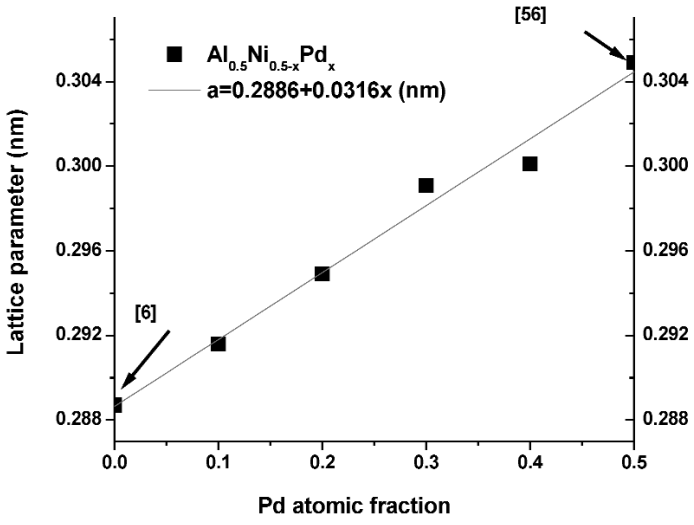

Fig. 17 Lattice parameters of $Al_{0.5}Ni_{0.5-x}Pd_x$ compounds.

Al–Ni–Cu

This system is unusual in that the extension of the B2 phase occurs along the composition line from NiAl to Cu_3Al. Recent work on the Al–Ni–Cu system shows that there is a B2 phase miscibility gap [57], and consequently one expects this should be reflected in the enthalpy of formation.

The B2 phase boundary at 1173 K in Fig. 18 shows that the B2 phase shifts to the Cu-rich range at the Al–Cu side. The enthalpies of formation of $Al_{0.4}Ni_{0.6-x}Cu_x$ ($0 \le x \le 0.45$) decreased with x increasing, which indicates the weaker bonding of Al–Cu and the B2 crystal structure is not stable at the composition AlCu. Figure 19 shows no indication of a positive deviation in the enthalpy as observed in the Al–Ni–Ru system.

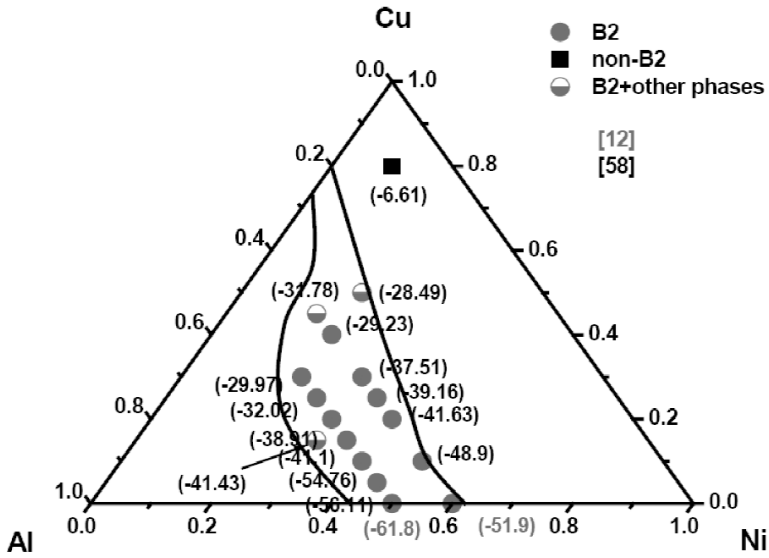

Fig. 18 Enthalpies of formation of Al–Ni–Cu compounds [58] and B2 phase boundary at 1173 K [59].

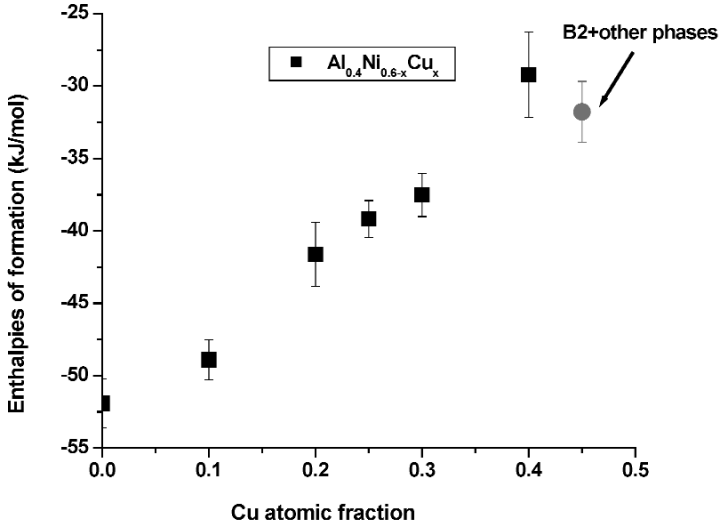

Fig. 19 Enthalpies of formation of $Al_{0.4}Ni_{0.6-x}Cu_x$ compounds.

Phases and lattice parameters of alloys in Al–Ni–Cu are summarized in Table 7. Lattice parameters of $Al_{0.5}Ni_{0.5-x}Cu_x$ compounds initially increased with x, but when x is larger than 0.20, Fig. 20, the lattice parameter becomes almost constant, which may indicate that these compositions are in a two-phase field. The lattice parameters of $Al_{0.4}Ni_{0.6-x}Cu_x$ increase, with x increasing in the single phase B2 region, Fig. 21.

Table 7 Phases and lattice parameters in the Al–Ni–Cu system.

Composition	Reaction enthalpy, ΔH_1 (kJ/mol)	Heat content, ΔH_2 (kJ/mol)	Enthalpy of formation ΔH_f (kJ/mol)	Phase	Lattice parameter of B2 phase (nm)
$Al_{0.5}Ni_{0.5}$			–61.8 ± 1.11 [12]	B2	0.2887
$Al_{0.5}Ni_{0.45}Cu_{0.05}$	–26.88 ± 0.87	29.23 ± 0.69	–56.11 ± 1.38	B2	0.2888
$Al_{0.5}Ni_{0.4}Cu_{0.1}$	–26.26 ± 0.66	28.5 ± 0.58	–54.76 ± 1.29	B2	0.2894
$Al_{0.5}Ni_{0.35}Cu_{0.15}$	–12.2 ± 0.87	28.9 ± 0.31	–41.1 ± 1.24	B2	0.2903
$Al_{0.5}Ni_{0.3}Cu_{0.2}$	–9.94 ± 1.00	28.97 ± 0.70	–38.91 ± 1.54	B2	0.2909
$Al_{0.5}Ni_{0.25}Cu_{0.25}$	0	32.02 ± 0.82	–32.02 ± 2.07	B2	0.2910
$Al_{0.5}Ni_{0.2}Cu_{0.3}$*	5.06 ± 1.4	35.03 ± 1.5	–29.97 ± 2.26	B2	0.2910
$Al_{0.40}Ni_{0.60}$			–51.9 ± 1.7 [12]	B2	0.2865 [6]
$Al_{0.40}Ni_{0.50}Cu_{0.10}$	–18.93 ± 0.62	29.97 ± 0.81	–48.90 ± 1.39	B2	0.2882
$Al_{0.40}Ni_{0.40}Cu_{0.20}$	–11.46 ± 1.86	30.17 ± 0.74	–41.63 ± 2.21	B2	0.2892
$Al_{0.40}Ni_{0.35}Cu_{0.25}$	–8.07 ± 0.56	31.09 ± 0.77	–39.16 ± 1.26	B2	0.2895
$Al_{0.40}Ni_{0.30}Cu_{0.30}$	–6.45 ± 1.07	31.06 ± 0.45	–37.51 ± 1.50	B2	0.2895
$Al_{0.40}Ni_{0.20}Cu_{0.40}$	4 ± 0.36	33.23 ± 0.63	–29.23 ± 1.19	B2	0.2901
$Al_{0.40}Ni_{0.15}Cu_{0.45}$	6.75 ± 1.41	38.53 ± 1.35	–31.78 ± 2.12	Not single B2	0.290
$Al_{0.55}Ni_{0.30}Cu_{0.15}$	–8.37 ± 0.95	33.06 ± 0.93	–41.43 ± 1.56	B2 + Al_3Ni_2	–
$Al_{0.10}Ni_{0.10}Cu_{0.80}$	29.48 ± 0.79	36.09 ± 1.12	–6.61 ± 1.60	(Ni, Cu)	–
$Al_{0.3}Ni_{0.20}Cu_{0.5}$	9.95 ± 0.70	38.44 ± 2.71	–28.49 ± 2.95	B2 + A4	–

*With small amount of non-B2 phase.

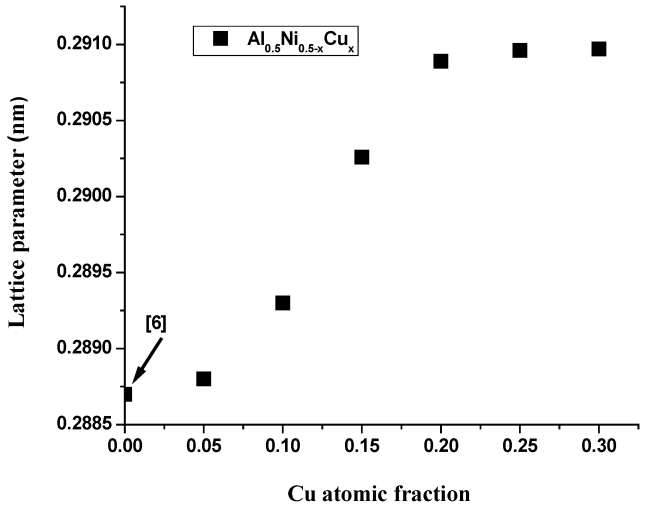

Fig. 20 Lattice parameters of $Al_{0.5}Ni_{0.5-x}Cu_x$ compounds.

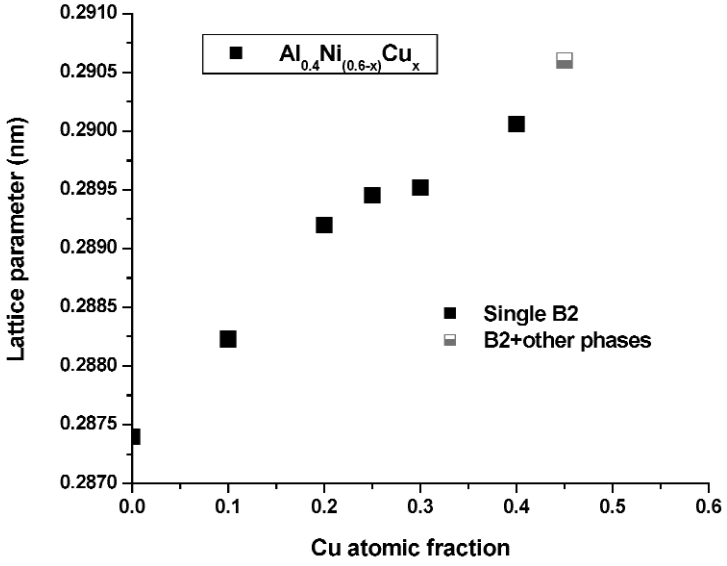

Fig. 21 Lattice parameters of $Al_{0.4}Ni_{0.6-x}Cu_x$ compounds.

Heat content and capacity

The heat content of the $Al_{0.5}Ni_{0.35}Cu_{0.15}$ alloy between room temperature and high temperatures (from 1243 to 1470 K) was measured with the calorimeter, Fig. 22. The heat capacities were calculated over this temperature range by fitting the heat content linearly, resulting in 27.7 J/mol/K. which is close to the value of 33.2 J/mol/K estimated using the Neumann–Kopp rule and slightly lower than the value of $Ni_{0.5}Al_{0.5}$, which is about 30.5 J/mol/K. This is reasonable since the heat capacity of Cu is smaller than Ni in this temperature range.

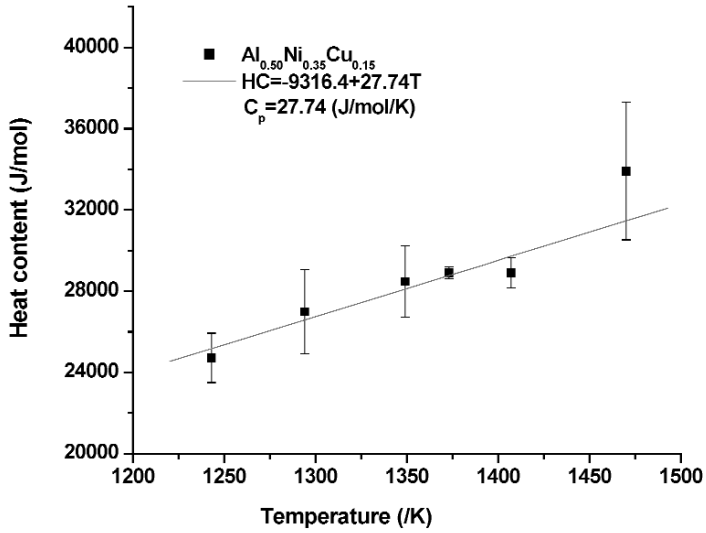

Fig. 22 Heat content and heat capacity of $Al_{0.5}Ni_{0.35}Cu_{0.15}$ at high temperature.

CONCLUSIONS

Atomic volume calculations in the Al–Ni–Fe system verify the constitutional defect site preference of Fe for the Al sublattice.

Comparisons of experimental data with the Miedema model and interpolation models show that any of the interpolation models will provide a more accurate prediction of the enthalpy of formation in a ternary system, assuming that the binary values are known accurately. No one interpolation model showed consistently more reliable predictions than any other.

The heat capacities of $Al_{0.5}Ni_{0.35}Cu_{0.15}$ and $Al_{0.5}Ni_{0.2}Ru_{0.3}$ were determined to be 27.74 and 27.2 J/mol/K, respectively.

When adding Cu, Pd, or Pt to NiAl, the lattice parameter of the B2 phase increases.

In the Al–Ni–Pd system, the B2 phase extends across the ternary system from NiAl to PdAl.

ACKNOWLEDGMENTS

We wish to thank the National Science Foundation under grants DMR 0209624 and DMR 0600690 for funding this work, Dr. Susan Meschel for her help in collecting the bibliography for this work and numerous discussions and advice regarding calorimeter experiments, Dr. Qiti Guo for help in maintenance and operation of the calorimeter, and Prof. Ole Kleppa for providing the inspiration for this work.

REFERENCES

1. P. Villars, A. Prince, H. Okamoto. *Handbook of Ternary Alloy Phase Diagrams* (computer file), ASM International, Materials Park, OH (1997).
2. T. B. Massalski, H. Okamoto, P. R. Subramanian, L. Kacprzak, W. W. Scott Jr. *Binary Alloy Phase Diagrams*, 2nd ed., ASM International, Materials Park, OH (1990).
3. F. Mücklich, N. Ilić. *Intermetallics* **13**, 5 (2005).
4. C. L. Fu. *Phys. Rev. B* **32**, 3151 (1995).
5. H. Araki, T. Mimura, P. Chalermkarnnon, M. Mizuno, Y. Shirai. *Mater. Trans., JIM* **43**, 1498 (2002).

6. R. D. Noebe, R. R. Bowman, M. V. Nathal. Review of the Physical and Mechanical Properties and Potential Applications of the B2 Compound NiAl, NASA Technical Memorandum 105598, 1992.
7. S. J. Suh, M. Dollar, P. Nash. *Mater. Sci. Eng., A* **192/193**, 691 (1995).
8. S. H. Kim, M. H. Oh, D. M. Wee. *Metall. Trans. A* **34**, 2089 (2003).
9. X. Y. Cheng, X. J. Wan, J. T. Guo, C. T. Liu. *Scripta Mater.* **38**, 959 (1998).
10. R. Kainuma, X. J. Liu, I. Ohnuma, S. M. Hao, K. Ishida. *Intermetallics* **13**, 655 (2005).
11. W. Huang, Y. A. Chang. *Intermetallics* **6**, 487 (1998).
12. P. Nash, O. Kleppa. *J. Alloys Compd.* **321**, 228 (2001).
13. J. Breuer, A. Grün, F. Sommer, E. J. Mittemeijer. *Metall. Trans. B* **32**, 913 (2001).
14. N. Bornsen, G. Bester, B. Meyer, M. Fahnle. *J. Alloys Compd.* **308**, 1 (2000).
15. M. Fähnle, B. Meyer, G. Bester, J. Majer, N. Börnsen. *Defect Diffusion Forum* **194–199**, 279 (2001).
16. V. Kuznetsovy, K. Tsaiz, T. Turkebaevz. *J. Phys.: Condens. Matter* **10**, 8957 (1998).
17. R. L. Fleischer. *J. Mater. Res.* **8**, 59 (1993).
18. H.-N. Su, P. Nash, Z. K. Liu. "Enthalpies of Formation of Alloys in the Al-Ni-Fe System", in *High Temperature Corrosion and Materials Chemistry*, IV, E. Opila, P. Hou, E. Wuchina, B. Pieraggi, T. Maruyama (Eds.), Electrochemical Society, Inc., Pennington, NJ (2003).
19. H. N. Su, P. Nash. *J. Alloys Compd.* **403**, 217 (2005).
20. G. Ghosh, M. Asta. *Acta Mater.* **53**, 3225 (2005).
21. C. Jiang, M. F. Besser, D. J. Sordelet, B. Gleeson. *Acta Mater.* **53**, 2101 (2005).
22. N. Stefanou, R. Zeller, P. H. Dederichs. *Phys. Rev. B* **35**, 2705 (1987).
23. B. D. Cullity, S. R. Stock. *Elements of X-ray Diffraction*, 3rd ed., Prentice Hall, Upper Saddle River, NJ (2001).
24. J. P. Neumann. *Acta Metall.* **28**, 1165 (1980).
25. L. M. Pike, Y. A. Chang, C. T. Liu. *Acta. Mater.* **45**, 3709 (1997).
26. L. M. Pike, I. M. Anderson, C. T. Liu, Y. A. Chang. *Acta Mater.* **50**, 3859 (2002).
27. S. V. Meschel, O. J. Kleppa. In *Metallic Alloys: Experimental and Theoretical Perspectives*, J. S. Faulkner, R. G. Jordan (Eds.), pp. 103–112, Kluwer Academic, Dordrecht (1994).
28. R. Hultgren, P. D. Desai, D. T. Hawkins, M. Gleiser, K. K. Kelley. *Selected Values of Thermodynamics Properties of Binary Alloys*, ASM International, Materials Park, OH (1973).
29. O. Kubaschewski, G. Heymer. *Trans. Faraday Soc.* **56**, 473 (1960).
30. R. Hu, P. Nash. *J. Mater. Sci. Lett.* **40**, 1067 (2005).
31. A. P. Bayanov. *Russ. J. Phys. Chem.* **45**, 1077 (1971).
32. W.-G. Jung, O. J. Kleppa. *Metall. Mater. Trans. B* **23**, 53 (1992).
33. W.-G. Jung, O. J. Kleppa. *J. Alloys Compd.* **176**, 309 (1991).
34. F. R. de Boer, D. G. Pettifor. *Cohesion in Metals*, Vol. 1, North-Holland, Amsterdam (1988).
35. N. Selhaoui, O. J. Kleppa. *J. Alloys Compd.* **191**, 145 (1993).
36. Q. Guo, O. J. Kleppa. *J. Alloys Compd.* **269**, 181 (1998).
37. C. Colinet, A. Pasturel, K. H. J. Buschow. *J. Appl. Phys.* **62**, 3712 (1987).
38. J. N. Pratt, J. M. Bird, S. Martosudirdjo. Rep. U.S. Army, Contr. DAJA 37-73-C-3010, Univ. of Birmingham, UK (1974).
39. C. R. Kao, L. M. Pike, S.-L. Chen, Y. A. Chang. *Intermetallics* **2**, 235 (1994).
40. Y. A. Chang, J. P. Neumann. *Prog. Solid State Chem.* **14**, 211 (1982).
41. H. Bakker. *Enthalpies in Alloys: Miedema's Semi-empirical Model*, Trans. Tech. Publications (1998).
42. M. Hillert. *Calphad* **4**, 1 (1980).
43. F. Kohler. *Monatsh. Chem.* **91**, 738 (1960).
44. I. Ansara. *Mater. Res. Soc. Symp. Proc.* **19**, 107 (1983).
45. Y. M. Muggianu, M. Gambino, J. P. Bros. *J. Chim. Phys.* **72**, 83 (1975).

46. G. W. Toop. *Trans. AIME* **233**, 850 (1965).
47. S. V. Meschel, O. J. Kleppa. *J. Alloys Compd.* **197**, 75 (1993).
48. S. V. Meschel, O. J. Kleppa. *J. Alloys Compd.* **191**, 111 (1993).
49. P. Nash. *Phase Diagrams of Binary Nickel Alloys*, ASM International, Materials Park, OH (1991).
50. L. Kaufman, H. Nesor. *Metall. Trans.* **5**, 1623 (1974).
51. H. N. Su. *Thermodynamic Modeling of Al and Ni Based Ternary Alloys*, Ph.D. dissertation, Illinois Institute of Technology, Chicago, Dec. 2004.
52. I. J. Horner, N. Hall, L. A. Cornish, M. J. Witcomb, M. B. Cortie, T. D. Boniface. *J. Alloys Compd.* **264**, 173 (1998).
53. I. Vjunitsky, E. Schonfeld, T. Kaiser, W. Steurer, V. Shklover. *Intermetallics* **13**, 35 (2005).
54. K. Rzyman, Z. Moser, A. P. Miodownik, L. Kaufman, R. E. Watson, M. Weinert. *Calphad* **24**, 309 (2000).
55. M. R. Jackson, J. R. Rairoden. "Protective coatings for superalloys and the use of phase diagrams", NBS, National Bureau of Standards, special publications, SP-496, Applications of phase diagrams in metallurgy and ceramics, proceedings of workshop, Gaithersburg, MD 1977 (498), 423 (1978).
56. P. Villars, L. D. Calvert. *Pearson's Handbook of Crystallographic Data for Intermetallic Phases*, Vol. 1, ASM International, Materials Park, OH (1985).
57. R. Kainuma, X. J. Liu, I. Ohnuma, S. M. Hao, K. Ishida. *Intermetallics* **13**, 655 (2005).
58. R. Hu, P. Nash. *J. Mater. Sci.* **41**, 631 (2006).
59. W. Köster, U. Zwicker, K. Moeller. *Zeit. Metall.* **39**, 225 (1948).